Direct measurement of the dispersion relation of capillary waves by laser interferometry

F. Behroozi and A. Perkins[a)]
Department of Physics, University of Northern Iowa, Cedar Falls, Iowa 50614

(Received 21 February 2006; accepted 25 May 2006)

Surface waves on fluids with wavelengths in the millimeter range are known as capillary waves. Surface tension determines the propagation and dispersion of capillary waves while gravity plays a minor role. We describe a simple method for generating standing capillary waves of known frequency on water and introduce a novel noncontact technique based on laser interferometry to measure the wavelength of capillary waves with great precision. The data gives the dispersion relation of capillary waves and provides an accurate method for determining the surface tension of fluids. © *2006 American Association of Physics Teachers.*
[DOI: 10.1119/1.2215617]

I. INTRODUCTION

Surface waves on water may be divided into two regimes. The familiar waves on lakes and oceans, with wavelengths ranging from hundreds of meters to a few centimeters, are called gravity waves. As the name implies, the dominant restoring force is gravity, which returns the disturbed surface of the water to equilibrium. Waves with wavelengths of a few millimeters and less are known as capillary waves. In this regime the dominant restoring force is the surface tension, which tends to minimize the surface area by smoothing out any wrinkles. Waves with intermediate wavelengths are known as capillary-gravity waves where gravity and surface tension play comparable roles.

It is difficult to obtain reliable experimental data for the dispersion of capillary waves because of the difficulty of measuring the wavelength and frequency of these miniature waves with the required precision. The most common method has been photon correlation spectroscopy,[1–3] where one analyzes line broadening of scattered light from thermally excited capillary waves to extract dispersion and attenuation data.[4–9] The usefulness of light scattering is limited because it is most suitable for studying capillary waves with wavelengths in the submicrometer range. Furthermore, recent studies show a significant reduction of surface energy of liquid interfaces at submicrometer length scales.[10] Because surface tension governs the dispersion of capillary waves, the dispersion data from light scattering is greatly affected by the reduction of surface tension at the very short wavelengths associated with thermally excited waves.

Because surface waves on fluids are very familiar to most undergraduates and fascinating, the experimental study of capillary waves is of interest and provides an excellent opportunity to study hydrodynamics. Unfortunately, apart from the limitations of the technique, the equipment for surface light scattering is complex and expensive.[11–14] Several recent attempts have been made to devise scaled down versions of the research instrumentation for use by undergraduates,[15,16] but the inherent limitations of the light scattering technique have limited widespread adoption of the method.

In this paper we describe a relatively simple noncontact method for the generation of standing capillary waves of known frequency in the millimeter wavelength regime and discuss a new technique for measuring their wavelength using a miniature laser interferometer with an uncertainty of about 0.1%. The wavelength data provide a very reliable dispersion relation, which yields accurate values of the phase and group velocities for capillary waves and the fluid surface tension.

The general properties of surface waves and the special characteristics of standing capillary waves are reviewed in Sec. II. We also give a new derivation of the dispersion relation, which exploits the conservation of energy as applied to standing waves. In Sec. III we introduce the technique for generating the standing capillary waves and discuss the interferometric technique for measuring their wavelengths. The results are discussed in Sec. IV.

II. THEORETICAL BACKGROUND

Low amplitude harmonic waves on deep water are circular.[17,18] Consider the case of capillary waves on the free surface of a lake. For convenience we choose a coordinate system in which the free equilibrium surface of the lake forms the x-z plane and the y axis is along the vertical. A right-circular wave traveling in the $+x$ direction is represented by

$$\boldsymbol{\psi}_1 = ae^{ky}[-\sin(kx-\omega t)\boldsymbol{i} + \cos(kx-\omega t)\boldsymbol{j}], \tag{1}$$

where $\boldsymbol{\psi}_1$ represents the displacement of a fluid element whose equilibrium position in the absence of the wave is at point (x,y); a is the wave amplitude, ω is the angular frequency, $k=2\pi/\lambda$ is the wave number with λ as the wavelength, and $\boldsymbol{i}$ and $\boldsymbol{j}$ are the unit vectors along the x and y axes. Note that $\boldsymbol{\psi}_1$ does not depend on z and the wave amplitude diminishes exponentially with depth below the surface. At a depth equal to one wavelength, the wave amplitude is less than 0.2% of the amplitude at the surface. Consequently the water is considered deep when its depth is greater than one wavelength. The condition for a low amplitude wave is satisfied when $a \ll \lambda$.

The velocity of a fluid element whose equilibrium position is at (x,y) is given by

$$\mathbf{v}_1 = \partial\boldsymbol{\psi}_1/\partial t = a\omega e^{ky}[\cos(kx-\omega t)\mathbf{i} + \sin(kx-\omega t)\mathbf{j}]. \tag{2}$$

Figure 1 is a representation of a right-handed circular wave traveling along the positive x direction with the phase speed ω/k. The amplitude of the wave has been exaggerated for clarity. The dashed arrows show the displacement of several fluid elements from their equilibrium positions; the solid arrows represent the velocity of these same fluid elements.

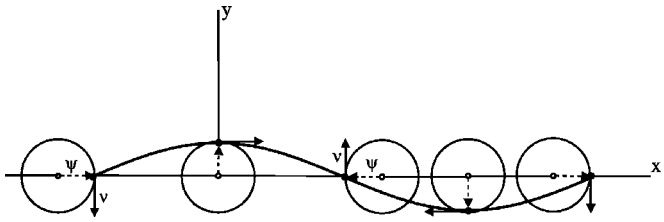

Fig. 1. Schematic representation of a traveling water wave as described by Eqs. (1) and (2). The amplitude of the wave has been exaggerated for clarity. The solid arrows represent the velocity of several water elements; the dashed arrows show the displacement of the same water elements from their equilibrium positions. Each water element moves with speed $a\omega e^{ky}$ in a clockwise direction around the circular path of radius ae^{ky}, centered on its equilibrium position (x,y), once every cycle.

Each fluid element moves clockwise with speed $a\omega$ along a circular path of radius a, centered on its equilibrium position (x,y), once every cycle. Similarly, a left-circular wave $\boldsymbol{\psi}_2$ traveling in the $-x$ direction may be represented by

$$\boldsymbol{\psi}_2 = ae^{ky}[-\sin(kx+\omega t)\mathbf{i} + \cos(kx+\omega t)\mathbf{j}]. \tag{3}$$

A. Standing waves

The superposition of $\boldsymbol{\psi}_1$ and $\boldsymbol{\psi}_2$ results in a standing wave given by

$$\boldsymbol{\psi} = \boldsymbol{\psi}_1 + \boldsymbol{\psi}_2 = 2ae^{ky}\cos\omega t[(\cos kx)\mathbf{j} - (\sin kx\ \mathbf{i}] \tag{4}$$

$$\mathbf{v} = \partial\boldsymbol{\psi}/\partial t = -2a\omega e^{ky}\sin\omega t[(\cos kx)\mathbf{j} - (\sin kx)\mathbf{i}]. \tag{5}$$

At the surface where $y=0$, Eq. (4) reduces to

$$\boldsymbol{\psi} = 2a\cos(\omega t)\mathbf{j}, \tag{6}$$

for $x=0, \pm\lambda/2, \pm 2\lambda/2, \ldots \pm n\lambda/2$, $n=0,1,2,3,\ldots$ The displacement $\boldsymbol{\psi}$ has only a vertical component at these values of x, which mark the lines of antinodes. That is, on the surface points along these lines, which run parallel to the z axis, water moves up and down with amplitude $2a$. For the corresponding points below the surface, the amplitude is reduced exponentially and is given by $2ae^{ky}$.

For the surface points for which $x=\pm\lambda/4$, $\pm 3\lambda/4, \ldots \pm(2n+1)\lambda/4$, $n=0,1,2,3,\ldots$, Eq. (4) reduces to

$$\boldsymbol{\psi} = 2a\cos(\omega t)\mathbf{i}, \tag{7}$$

indicating that $\boldsymbol{\psi}$ is purely horizontal at these points, that is, the fluid elements move back and forth parallel to the surface with amplitude $2a$. Again, directly below these points the displacement amplitude is modulated by the e^{ky} factor.

At points other than the nodes and antinodes water elements moves at an angle to the vertical as is evident from Eq. (4). For example, at $x=\pm\lambda/8, \pm 3\lambda/8$, the water elements move at $\pm 45^\circ$ to the vertical.

B. Dispersion relation

Most texts on hydrodynamics obtain the dispersion relation of capillary-gravity waves by applying the boundary condition at the free surface to the velocity potential.[19–22] In recent years several alternative approaches have appeared to make the derivations more accessible to undergraduates.[23–26]

Here we present the outline of a new and more intuitive derivation of the dispersion relation, based on conservation of energy.[27] Consider a region of deep water on which a standing capillary wave has been established. Equations (4) and (5) describe the resulting standing wave. Recall that $\boldsymbol{\psi}(x,y,t)$ and $\boldsymbol{v}(x,y,t)$ give at time t the displacement and velocity of a water element whose equilibrium position is at point (x,y). According to Eq. (5), at time $t=0$ the standing wave is stationary. Hence the displacement is a maximum and thus the entire energy of the wave is in potential form, partly gravitational and partly surface energy. A quarter period later, when $t=\tau/4=\pi/2\omega$, the displacement is zero but the velocity attains its maximum value. So at $t=\tau/4$ the entire energy of the wave is kinetic. Conservation of energy demands that the potential energy at $t=0$ should equal the kinetic energy at $t=\pi/2\omega$. This observation yields the desired expression for the dispersion of surface waves.

In particular, at $t=0$, when the entire energy is potential, the gravitational potential energy part of the wave per unit surface area is given by $U_g=g\rho a^2$, where ρ is the fluid density and g is the gravitational acceleration. The potential energy per unit area residing in the excess surface generated by the wave is given by $U_s=a^2k^2\sigma$, where σ is the surface tension. So at $t=0$, the total energy of the wave per unit area is

$$E_t = U_g + U_s = g\rho a^2 + a^2k^2\sigma. \tag{8}$$

At $t=\tau/4=\pi/2\omega$, the entire wave energy is kinetic. The energy per unit area is given by[27]

$$E_t = \rho a^2\omega^2/k. \tag{9}$$

If we equate Eqs. (8) and (9) for the total energy, $\rho a^2\omega^2/k = g\rho a^2 + a^2k^2\sigma$, we obtain the well-known dispersion relation for surface waves,

$$\omega^2 = gk + k^3\sigma/\rho. \tag{10}$$

In light of Eq. (8), when the entire wave energy is in potential form, the ratio of the surface energy to the gravitational energy may be written as

$$U_s/U_g = k^2\sigma/g\rho. \tag{11}$$

Equation (11) implies that the gravitational and surface energies are equal at a special wave number k^*, where

$$k^* = (g\rho/\sigma)^{1/2}. \tag{12}$$

The corresponding wavelength $\lambda^* = 2\pi/k^* = 2\pi(\sigma/g\rho)^{1/2}$ is the wavelength at which both gravity and surface tension play equal roles.

C. Phase and group velocities

Equation (10) may be used to obtain the phase and group velocities of surface waves. Thus,

$$v_\varphi = \omega/k = (g/k + \sigma k/\rho)^{1/2}, \tag{13}$$

and

$$v_G = d\omega/dk = (1/2)[(g+3\sigma k^2/\rho)/(gk+\sigma k^3/\rho)^{1/2}]. \tag{14}$$

In Fig. 2 we plot the phase and group velocities as functions of the wavelength. Note that the wavelength scale is logarithmic to accommodate both capillary and gravity waves. The two graphs cross when the phase and group velocities become equal, that is, when $v_\varphi = v_G$. Not surprisingly, if we equate Eqs. (13) and (14) we obtain $k^* = (g\rho/\sigma)^{1/2}$, or

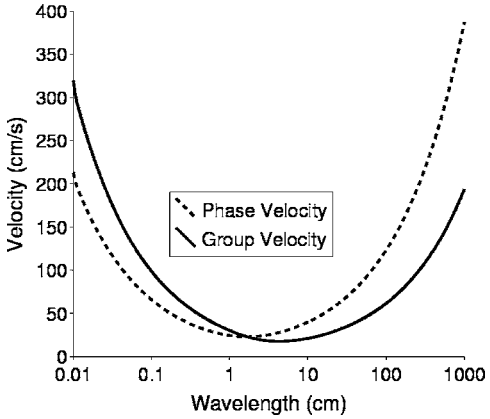

Fig. 2. Phase and group velocities of water waves as functions of the wavelength. Note that at the special wavelength of 1.70 cm the two velocities have the same value (23 cm/s).

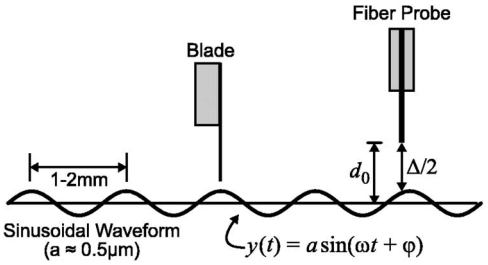

Fig. 3. Schematic of a fiber-optic probe and a wave-generating blade above the fluid surface.

$$\lambda^* = 2\pi(\sigma/\rho g)^{1/2}. \tag{15}$$

For pure water at 20 °C $\lambda^* = 1.7$ cm. At this wavelength, $v_\varphi = v_G = (4g\sigma/\rho)^{1/4} = 23$ cm/s. A related parameter, the capillarity length, is defined by the expression $\zeta \equiv 1/k^* = \lambda^*/2\pi = (\sigma/g\rho)^{1/2}$. For pure water $\zeta = 0.27$ cm.

Another feature of the graphs in Fig. 2 is that for capillary waves, the group velocity exceeds the phase velocity. For very short wavelength capillary waves with $k^2 \gg \rho g/\sigma$, Eqs. (13) and (14) may be approximated to give

$$v_\varphi \cong (\sigma k/\rho)^{1/2}, \tag{16a}$$

$$v_G \cong 3/2(\sigma k/\rho)^{1/2} = 3/2 v_\varphi. \tag{16b}$$

For capillary waves the group velocity is 3/2 times that of the phase velocity. As mentioned, in this wavelength regime the surface tension is the dominant restoring force. In other words, because $k^2 \gg \rho g/\sigma$, we may neglect the gravity term in the dispersion relation to obtain

$$\omega^2 \cong \sigma k^3/\rho. \tag{17}$$

Equation (17) can be recast into the Kelvin equation, which relates the surface tension of a fluid to the frequency and wavelength of the capillary waves,

$$\sigma \cong \rho\omega^2/k^3. \tag{18}$$

In the long wavelength regime we may neglect the surface tension term because $k^2 \ll \rho g/\sigma$. In this case Eqs. (13) and (14) give

$$v_\varphi \cong (g/k)^{1/2}, \tag{19a}$$

$$v_G \cong 1/2(g/k)^{1/2} = 1/2 v_\varphi. \tag{19b}$$

For gravity waves the phase velocity is twice the group velocity.

III. EXPERIMENTAL TECHNIQUE

The experimental technique has been described in detail in Refs. 28–30. Here we present a summary. A Teflon trough (6 cm × 46 cm, with a depth of 1 cm) is used to contain the fluid of interest. Thermoelectric cells underneath the trough regulate the temperature. To minimize air currents and mechanical disturbances, the experimental system is housed in an enclosure and placed on an isolation table.

Capillary waves are generated electronically by placing a metallic blade a few tenths of a millimeter above the fluid surface. A dc-biased sinusoidal voltage of a few hundred volts at a selected frequency is applied between the blade and the fluid. For polar fluids such as water or water based binary fluids, the alternating electric field under the blade generates two capillary wave trains that recede from the blade on each side. Typically the amplitude of these waves is of the order of one micrometer.

The capillary waves are detected by using a fiber-optic system which functions as a miniature laser interferometer. The heart of the system consists of a single mode optical fiber, one end of which is positioned a short distance above the fluid surface (see Fig. 3). Laser light traveling through the optical fiber is partially reflected from the cleaved tip of the fiber and again from the fluid surface. The two reflected beams travel back through the same fiber and generate an interference signal at the detector. As the fluid level under the probe changes due to the wave motion, the gap between the fiber tip and the fluid surface changes causing a periodic change in the path difference. Thus, the number of fringes in the periodic interference signal gives an accurate measure of the wave amplitude.

Figure 3 is a schematic of one wave generating blade and a fiber probe. The fiber-optic probe is mounted on an electronic micrometer that records the probe position on the surface with an accuracy of about one μm. The distance from the tip of the probe to the equilibrium surface is d_0, and the roundtrip distance between the tip of the probe and the fluid surface, that is, the path difference between the two reflected beams, is Δ. A typical wavelength is about one millimeter, and a typical wave amplitude is less than one micrometer. The wave amplitude has been vastly exaggerated for clarity in Fig. 3.

A schematic of the optoelectronic system is shown in Fig. 4. Part of the laser light is split by the cube splitter and used as a reference signal at the detector to compensate for any laser output fluctuations. The main beam passes through a birefringent cube and is split into two equal beams for use in the two fiber-optic probes. The Gould multiplexer is essential in routing the interference signal to the detector and preventing the signal from returning back to the laser. The Faraday rotator further isolates and protects the laser cavity from "seeing" any reflected signal.

The interference signal is detected, amplified, and digitized for later analysis. The raw interference signal for a half period is shown at the top of Fig. 5. The solid curve repre-

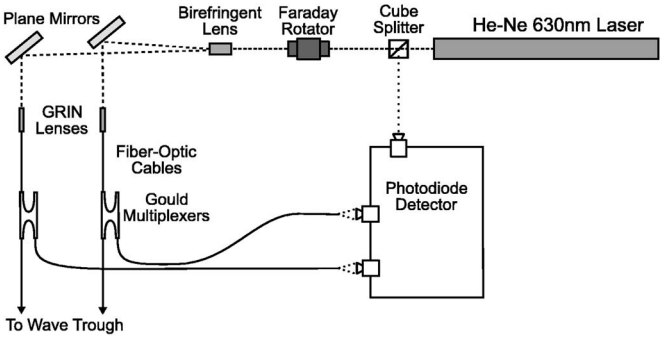

Fig. 4. Schematic of the optical and electronic detection system. The Gould multiplexer is essential for routing the interference signal to the detector. The Faraday rotator isolates and protects the laser cavity from any reflected signal.

sents the fit, which replicates the trace faithfully. The dashed curve gives the vertical displacement of the surface wave under the probe as a function of time.

There is a one to one correspondence between the surface wave amplitude and the resulting interference pattern. As discussed in Ref. 31, the number of fringes in the interference pattern for a half period is proportional to the wave amplitude under the probe. In a half period, the fluid surface under the probe suffers a displacement of $2a$ as the wave trough follows the wave crest. The corresponding change in the path difference between the two reflecting beams is $4a$. Thus the number of fringes for a half-period in the interference pattern is $4a/\lambda_l$, where λ_l is the wavelength of the laser light. For the pattern shown in Fig. 5 the number of fringes is 6.78. Because the wavelength of the He-Ne laser used here is $\lambda_l=633$ nm, the amplitude of the wave is 1.07 μm.

A standing wave is generated when two waves of the same frequency and amplitude move in the same space but in opposite directions. Two generating blades are used to establish a standing capillary wave on the surface between the two blades. Each blade sends a wave train toward the other with the same amplitude and frequency. If the distance between the two blades D is chosen to be a half odd-integer wavelength, $D=(2n+1)\lambda/2$, then the two wave trains interfere destructively on the outer sides of the blades. This choice of

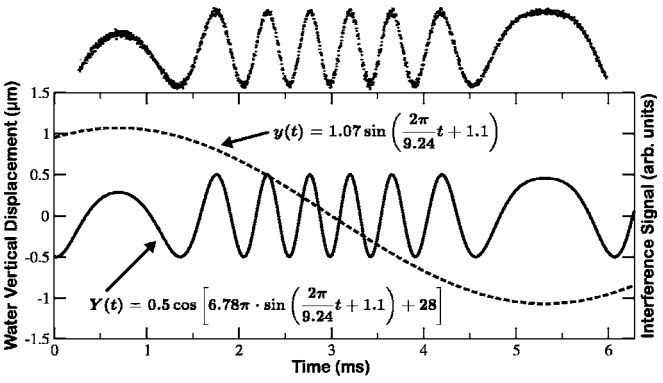

Fig. 5. The interference signal for one half wavelength. The raw interference signal for the half period is shown at the top of the frame. The solid curve is the fit, which replicates the trace faithfully. The dashed curve gives the vertical displacement of the surface wave under the probe as a function of time. The right scale is for the interference signal and the left scale is for the wave amplitude.

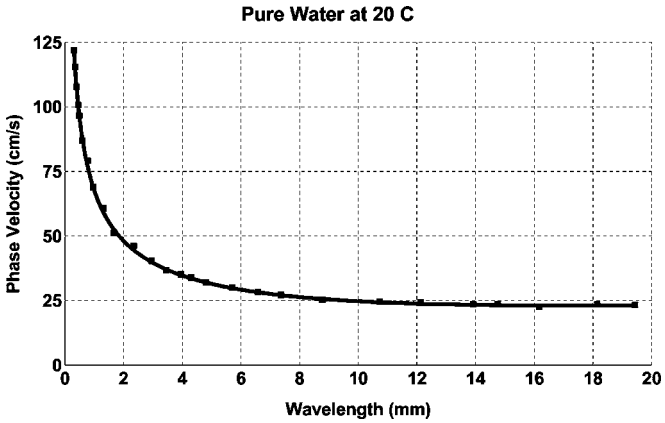

Fig. 6. Phase velocity of pure water vs wavelength at 20 °C. The solid line is the theoretical phase velocity using the surface tension value of 72.8±0.1 dyne/cm.

the blades' separation produces a region of standing waves between the blades while the surface outside the blades remains calm. One of the two probes is used to monitor the region outside the blades.

When a standing wave is established on the fluid surface between the two blades, the accurate measurement of the distance between several nodes determines the wavelength of the wave very accurately. We move one of the two fiber-optic probes over the surface, starting near one blade and moving toward the other. As the probe moves over nodes and antinodes, the interference fringe count peaks at an antinode and diminishes to zero over a node. Thus it is possible to count the number of nodes as the probe scans the surface. Because a digital micrometer monitors the probe's position, we can measure the wavelength of the standing capillary waves to within one μm.

IV. RESULTS AND DISCUSSION

In Fig. 6 we plot the experimental phase velocity $v_\varphi=f\lambda$ as a function of the wavelength λ at a temperature of 20 °C. Each data point is obtained by measuring the wavelength of the capillary wave at a given frequency. The solid line is the theoretical expression for the phase velocity given by

$$v_\varphi = (g/k + \sigma k/\rho)^{1/2}. \tag{20}$$

The parameters g, ρ, and $k=2\pi/\lambda$ are known; the surface tension σ is the only adjustable parameter. For the graph shown in Fig. 6, the best fit to the data points is obtained for $\sigma=72.8\pm0.1$ dyne/cm.

Although this way of extracting the experimental value of surface tension from the dispersion data is simple, there is a more convenient alternative. The dispersion relation may be recast in the form

$$\omega^2/k = g + \sigma k^2/\rho. \tag{21}$$

A plot of the experimental values of ω^2/k as a function of k^2 gives a linear graph with a slope of σ/ρ. Figure 7 shows the experimental data for pure water at 20 °C. The solid line is generated by plotting $(g+\sigma k^2/\rho)$ versus k^2 with σ as the only adjustable parameter. Not surprisingly, the best fit is obtained for $\sigma=72.8\pm0.1$ dyne/cm.

The dispersion data is temperature dependent because surface tension and density are functions of temperature. When

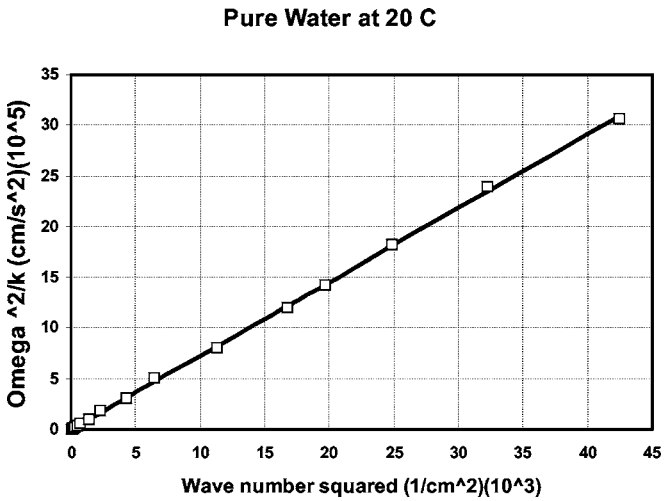

Fig. 7. The data points give the experimental values of ω^2/k vs k^2. The solid line is a plot of $(g+\sigma k^2/\rho)$ as a function of k^2 with σ as the adjustable parameter. The best fit is obtained for $\sigma=72.8\pm0.1$ dynes/cm.

the temperature dependence of the density is known, the temperature dependence of surface tension is easily measurable with our system. Our data at 25 °C is very similar to the data at 20 °C, except that the fit gives a value of $\sigma=72.0$ dyne/cm.

The measurement of surface tension has been of much interest for more than a century, and many ingenious experimental methods have been devised.[32,33] The most intuitive method is the pull method, which measures the force needed to pull a suitable object out of the fluid surface and relates the pull force to the surface tension. The most commonly used versions of the pull method are the Wilhelmy plate and the du Nouy ring methods. These versions are simple in principle, but are prone to measurement errors due to the uncertainty introduced by the difficulty of measuring the contact angle at the solid liquid interface accurately. Often a platinum plate or a platinum-iridium ring is used to minimize the effect of the contact angle variation. In practice the plate or the ring must be fire cleansed just before taking a measurement to allow one to assume a zero contact angle. Often it is necessary to apply certain correction factors to obtain good results.[32]

In contrast, our method introduces no correction factor or unknown parameter and gives the surface tension without any instrumental contact with the surface. Because surface contamination is a major cause of error in determining the surface tension of fluids and particularly fluids covered by surfactant monolayers, the method described here provides a distinct advantage in this regard. However, our method works well only for polar fluids due to the fact that in our system capillary waves are generated by the action of an oscillating electric field between the blade and the fluid. Water works very well because it is a polar fluid. We have experienced no difficulty in obtaining dispersion data on binary mixtures of glycerin-water, acetone-water, and ethylene-water mixtures containing as little as 10% water. The method is also very suitable for measuring the surface tension when a surfactant or monolayer covers the water surface.

[a]Present address: Department of Physics, Georgia Institute of Technology, Atlanta, GA 30332.

[1] D. Langevin, *Light Scattering by Liquid Surfaces and Complementary Techniques* (Dekker, New York, 1992).
[2] J. C. Earnshaw, "Surface light scattering: A methodological review," Appl. Opt. **36**, 7583–7592 (1997).
[3] D. M. Buzza, "General theory for capillary waves and surface light scattering," Langmuir **18**, 8418–8435 (2002).
[4] R. H. Katyl and U. Ingard, "Line broadening of light scattered from liquid surface," Phys. Rev. Lett. **19**, 64–67 (1967).
[5] J. S. Huang and W. W. Webb, "Viscous damping of thermal excitations on the interface of critical fluid mixtures," Phys. Rev. Lett. **23**, 160–163 (1969).
[6] K. Y. Lee, T. Chou, D. S. Chung, and E. Mazur, "Capillary wave damping in heterogeneous monolayers," J. Phys. Chem. **97**, 12876–12878 (1993).
[7] C. Martel and E. Knobloch, "Damping of nearly inviscid water waves," Phys. Rev. E **56**, 5544–5548 (1997).
[8] P. Cicuta and I. Hopkinson, "Dynamic light scattering from colloidal fractal monolayers," Phys. Rev. E **65**, 041404-1–5 (2002).
[9] P. Cicuta and I. Hopkinson, "Recent development of surface light scattering as a tool for optical-rheology of polymer monolayers," Colloids Surf., A **233**, 97–107 (2004).
[10] C. Fradin, A. Braslau, D. Luzet, D. Smilgies, M. Alba, N. Boudet, K. Mecke, and J. Daillant, "Reduction in surface energy of liquid interfaces at short length scales," Nature (London) **403**, 871–874 (2000).
[11] S. Hård, Y. Hamnerius, and O. Nilsson, "Laser heterodyne apparatus for measurements of liquid surface properties—Theory and experiment," J. Appl. Phys. **47**, 2433–2442 (1976).
[12] K. J. Måløy, J. Feder, and T. Jøssang, "An experimental technique for measurement of capillary waves," Rev. Sci. Instrum. **60**, 481–486 (1989).
[13] B. J. A. Bjorkvik, D. Waaler, and T. Sikkeland, "A versatile interface light-scattering spectrometer," Meas. Sci. Technol. **6**, 1572–1581 (1995).
[14] P. Tin, J. A. Mann, W. V. Meyer, and T. W. Taylor, "Fiber-optics surface light scattering spectrometer," Appl. Opt. **36**, 7601 (1997).
[15] T. M. Jorgensen, "A low-cost surface laser light scattering spectrometer," Meas. Sci. Technol. **3**, 26–27 (1992).
[16] W. M. Klipstein, J. S. Radnich, and S. K. Lamoreaux, "Thermally excited liquid surface waves and their study through the quasielastic scattering of light," Am. J. Phys. **64**, 758–765 (1996).
[17] J. Lighthill, *Waves in Fluids* (Cambridge University Press, 1978), p. 208.
[18] F. Behroozi and N. Podolefsky, "Capillary-gravity waves and the Navier-Stokes equation," Eur. J. Phys. **22**, 587–593 (2001).
[19] T. E. Faber, *Fluid Dynamics for Physicists* (Cambridge University Press, 1995), p. 174.
[20] D. Pnueli and C. Gutfinger, *Fluid Mechanics* (Cambridge University Press, 1992), pp. 160–162.
[21] L. D. Landau and E. M. Lifshitz, *Fluid Mechanics*, 2nd ed. (Pergamon, New York, 1987), p. 245.
[22] Reference 17, p. 223.
[23] F. S. Crawford, "A simple model for water-wave dispersion relations," Am. J. Phys. **55**, 171–172 (1987).
[24] F. S. Crawford, "Ideal water waves via instantaneous action at a distance," Am. J. Phys. **56**, 300–303 (1988).
[25] F. S. Crawford, "Speed of gravity waves in deep water: Another elementary derivation," Am. J. Phys. **60**, 751–752 (1992).
[26] H. Georgi, *The Physics of Waves* (Prentice Hall, Englewood Cliffs, NJ, 1993), pp. 294–297.
[27] F. Behroozi and N. Podolefsky, "Dispersion of capillary-gravity waves: a derivation based on conservation of energy," Eur. J. Phys. **22**, 225–231 (2001).
[28] F. Behroozi, B. Lambert, and B. Buhrow, "Direct measurement of the attenuation of capillary waves by laser interferometry: Non-contact determination of viscosity," Appl. Phys. Lett. **78**, 2399–2402 (2001).
[29] F. Behroozi, B. Lambert, and B. Buhrow, "Noninvasive measurement of viscosity from damping of capillary waves," ISA Trans. **42**, 3–8 (2003).
[30] F. Behroozi, U.S. Patent No. 6,563,588 B2: "Apparatus and method for measurement of fluid viscosity" (13 May 2003).
[31] F. Behroozi and P. S. Behroozi, "Efficient deconvolution of noisy periodic interference signals," J. Opt. Soc. Am. A **23**, 902–905 (2006).
[32] K. S. Birdi, *Lipid and Biopolymer Monolayers at Liquid Interfaces* (Plenum, New York, 1989), pp. 32–37.
[33] A. W. Adamson, *Physical Chemistry of Surfaces*, 5th ed. (Wiley, New York, 1990), pp. 4–45.